INSTABILITY AND TRANSITION MECHANISMS IN LAMINAR SEPARATION BUBBLES

Ulrich Rist
Institut für Aerodynamik & Gasdynamik
Universität Stuttgart
Pfaffenwaldring 21
D-70550 Stuttgart, Germany

E-Mail: rist@iag.uni-stuttgart.de

ABSTRACT

The present paper is intended to give an introduction and an overview on instability and transition mechanisms found in generic pressure-induced laminar separation bubbles. These bubbles have been generated by imposing an external positive stream-wise pressure gradient on a laminar boundary layer flow along a smooth flat plate. Using velocity profiles extracted at various streamwise stations for a local stability analysis based on the *Orr–Sommerfeld* equation it is shown that linear primary instability is a valid tool to describe the initial disturbance development. Then, linear stability theory is used to clarify the competition between the so-called "Tollmien–Schlichting instability" of the boundary layer and the so-called "Kelvin–Helmholtz instability" of a mixing layer, followed by a further refinement of the border between 'convective' and 'absolute' instability. Non-linear scenarios are investigated by DNS. They show a dramatic influence of small upstream disturbances on the mean flow of the laminar separation bubble. Next, transition scenarios are investigated, analysed and compared to each other. It turns out that secondary instability doesn't play the same remarkable role as in an attached boundary layer. In fact, large-amplitude 2-D fluctuations can control the re-attachment process to a large extent. The fastest transition to turbulence is found to occur when moderately oblique waves interact with each other. This mechanism directly yields to small-scale turbulence, as well as longitudinal vortices in the re-attachment zone. For large enough laminar separation bubbles a new instability mechanism has been identified which amplifies small-amplitude 3-D disturbances in the re-attachment zone. Finally, the author's view on receptivity, flapping and the bubble bursting process is presented. Hence, the present investigations concentrate on different instability mechanisms and their possible contributions to laminar-turbulent transition in laminar separation bubbles based on research performed by the author.

1.0 INTRODUCTION

Laminar separation bubbles (*LSBs*) are a typical phenomenon of low Reynolds number aerodynamics. They may appear on aircraft like small unmanned aerial vehicles (UAVs), on the wings of man-carrying sail planes, on the vanes of turbo-machines, on the blades of wind-energy converters, and even on the slats of large commercial jet-powered airliners. A prerequisite for their occurrence is a laminar boundary layer facing a too large pressure rise in streamwise direction (i.e. an adverse pressure gradient), transition to turbulence of the separated shear layer

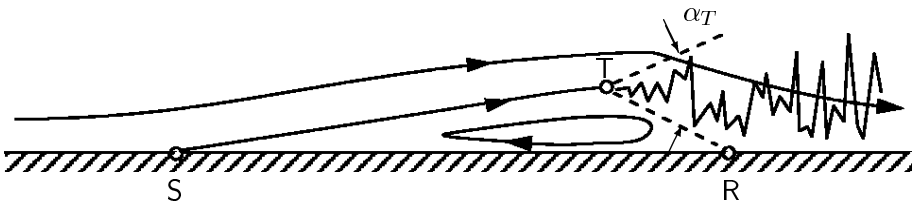

Figure 1: Schematic illustration of a transitional laminar separation bubble. S = laminar separation, R = re-attachment, T = transition, α_T = spreading angle of turbulence.

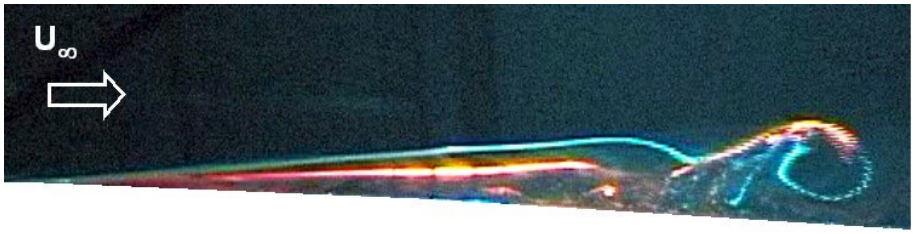

Figure 2: Snapshot visualisation of a laminar separation bubble in the water channel of IAG (Lang, 2002).

and re-attachment to the wall of the turbulent boundary layer. This is illustrated in Fig. 1. In such an idealized (or time-averaged) view one observes a separation point (S), a vortex inside the LSB and a transition point (T) with an ensuing turbulent wedge (α_T) that re-attaches to the wall at a re-attachment point (R).

An experimental realisation of a LSB is shown in Fig. 2 which has been taken in the so-called laminar water channel of our institute (IAG), which is a research facility for studying basic fluid dynamical problems [18]. Hydrogen bubbles have been generated by an electrically heated wire close to the wall upstream of separation and a dye called *Rhodamin* has been introduced into the separation bubble. With the help of a laser light sheet oriented in streamwise direction the main features become apparent. They consist of a separating laminar boundary layer[1], a separation zone underneath the detached shear layer, and an almost periodic vortex shedding at the downstream end of the bubble. Such a snapshot visualisation of the *instantaneous* flow field is in considerable contrast to the picture of the time averaged mean flow typically found in literature (e.g. Fig. 1). Strictly speaking the idealized picture of Fig. 1 never exists. The three main differences between the real flow and its idealization are the unsteady vortex shedding instead of a steady (turbulent) re-attachment, no definite transition point, nor a turbulent wedge, and a series of re-attachment and separation points that move downstream with the shed vortices which may be called the "coherent structures" of the turbulent boundary layer.

A sketch of the flow physics which are supposed to be present in a LSB is given in Fig. 3. Similar to boundary layer transition one assumes a receptivity process (1) which transforms free-stream disturbances, sound and roughness into boundary layer disturbances. Once present, these are amplified by linear stability (2) in the ensuing boundary layer which leaves the wall at 'S'. When they attain finite amplitudes, non-linear interactions (3) may take place leading to laminar-turbulent transition and in due course to a turbulent boundary layer after re-attachment. Due to the reverse flow near the wall an upstream feedback (4) of disturbances inside the LSB can be assumed as well.

[1] the term "free shear layer" typically found in literature is deliberately avoided here, because of the continuing influence of the wall after separation, see sec. 3.3

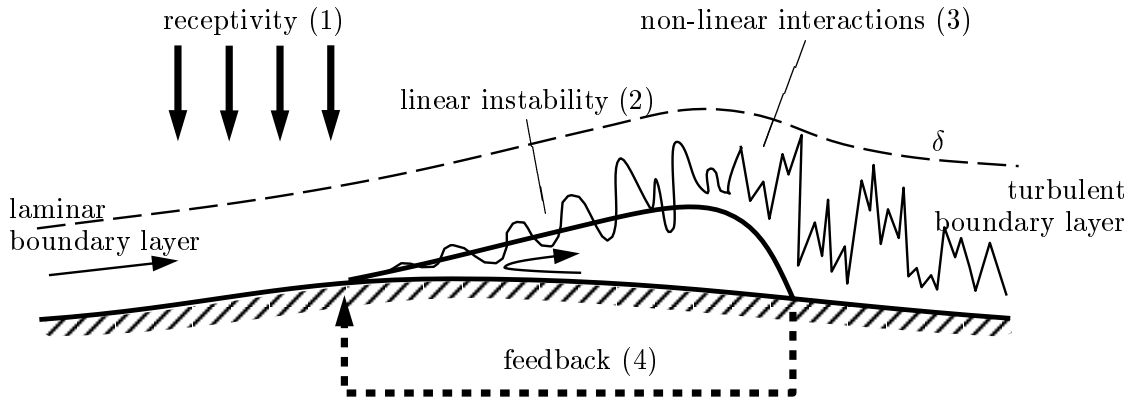

Figure 3: Instability and transition mechanisms in a laminar separation bubble after Dovgal *et al.*, 1994 [7].

The present paper will present an overview on recent (theoretical) research on laminar separation bubbles at IAG, University of Stuttgart. Only pressure-induced laminar separation bubbles that occur on a smooth surface will be treated. The reader who is interested to see whether similar effects occur in roughness-induced laminar separation bubbles (i.e., behind or in front of steps) may start with reviews like Tani (1964) [38], Dovgal *et al.* (2001) [7] or Boiko *et al.* (2001) [4] and the references therein. Especially the last two reviews contain many references to experimental work for pressure-induced LSBs, in particular from Russia.

The aim of the present contribution is to shed more light on the largely unknown instabilities of transitional laminar separation bubbles and their contribution to laminar-turbulent transition. As a rule, the reader should be aware that "the laminar separation bubble" as a unique or universal feature does not exist. Rather, each bubble depends on the characteristics of the arriving laminar boundary layer, the ensuing pressure gradient, and, not to the least, on the background disturbance level and spectrum of the incoming flow, as will be shown further down. In an attempt to control the influence of the disturbance background as far as possible, most of the present work is based on DNS with carefully selected disturbance combinations with the intention of isolating and understanding different mechanisms.

The paper is organized as follows. Section 2 introduces the numerical methods used, direct numerical simulation (DNS) and linear stability theory (LST). Key results are presented in section 3, starting with investigations of the linear (primary) instability of separation bubble flows, which also include the influence of the wall and an investigation of the border between absolute and convective instability. Using DNS the influence of disturbance amplitudes on bubble size is illustrated, followed by a comparison of different generic secondary instability scenarios, direct 3-D disturbance amplification due to oblique breakdown, and a newly found absolutely unstable secondary instability mechanism. The fourth section presents some LSB related aspects which have not yet been treated to the same depth as the previous ones. These are receptivity issues of a laminar separation bubble, 'flapping', and the issue of "bubble bursting". The fifth section presents the conclusions and an outlook.

2.0 METHODS OF INVESTIGATION

Because of the high sensitivity of the flow with respect to intrusive measurement techniques and the difficulties of computing the flow field via boundary-layer or Reynolds-averaged Navier–Stokes (RANS) equations, our research relies primarily on direct numerical simulations (DNS) based on the complete Navier–Stokes equations, backed by linear stability theory, wind tunnel

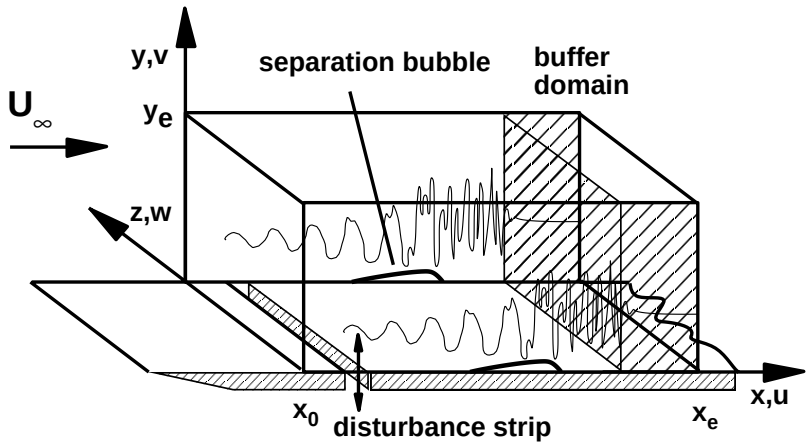

Figure 4: Integration domain for the DNS of instability and transition in a laminar separation bubble.

and (non-intrusive) water channel experiments. Using Laser-Doppler Anemometry (LDA) and Particle-Image Velocimetry (PIV) it is now possible to measure unsteady flow quantities without influencing the flow, but this will not be discussed further here. Other numerical methods, like RANS or Large-Eddy Simulation (LES) are not covered here, either. The first because it doesn't cover the unsteady flow physics, the second because it is not yet well proven for transitional flows.

2.1 DNS Method

We consider the incompressible flow over a portion of a flat plate with a free-stream pressure gradient specified at the upper boundary of the according integration domain ($y = y_e$, see Fig. 4). The coordinate system is chosen such that the coordinate x corresponds to the free-stream flow direction (along the flat plate), y is the direction normal to the plate, and z the spanwise direction. The according velocity components are called u, v, and w. The method described in [8, 32] and [23, 30] is used. It is based on a vorticity-velocity formulation of the Navier–Stokes equations, discretised by fourth-order accurate finite differences in x- and y-direction and a Fourier ansatz in z, i.e. periodicity with a prescribed wavelength λ_z is assumed in z. Time integration of the vorticity transport equation is performed via an explicit Runge-Kutta scheme of fourth-order accuracy. Here, DNS is used for two purposes: (i) to calculate a steady two-dimensional base flow that can be used for linear stability (cf. section 2.2), and (ii) to compute the unsteady three-dimensional disturbance flow that results from unsteady forcing at the boundaries of the integration domain.

To create a laminar separation bubble a steady laminar boundary layer is specified at the inflow boundary of the integration domain together with a function $U_p(x)$ at the free-stream boundary $y = y_e$. Typically, the latter contains a region of local adverse pressure gradient that causes the laminar boundary layer to separate and to re-attach a short distance further downstream (see Fig. 5 further down). In such a case, a steady two-dimensional base flow can be computed independently from the investigation of disturbances, as in [32] and [35]. However, for sufficiently large streamwise pressure gradients or high enough Reynolds numbers the flow becomes unsteady and splitting into a steady base flow and an unsteady disturbance flow is no longer possible. But this causes no severe problem since the computations are performed in an unsteady total-flow formulation then. Large displacements of the laminar separation bubble will

cause changes in the free-stream velocity at $y = y_e$. Based on the viscous-inviscid interaction model of Veldman [40], Maucher [23] has constructed a procedure to update $U_p(x)$ which allows to compute flow fields that are basically independent from y_e [23]. However, this feature is not used in the following computations.

Wall boundary conditions as in [32] and outflow conditions which contain the buffer domain of [17] complement the specification of the problem. The boundary conditions at the wall include the possibility to introduce disturbances via blowing and suction in a narrow disturbance strip placed upstream of the bubble. Within the strip the v'-velocity component is prescribed as a function of x, z, and t. This constitutes an elegant method to introduce any kind of unsteady, steady, two- or three-dimensional disturbances, or any combinations thereof [32]. Because of the assumption of spanwise symmetry any single harmonic, three-dimensional forcing will generate a pair of oblique waves.

2.2 Linear Stability Theory

In linear stability theory (LST) one works with a local and linearized version of the Navier–Stokes equations, the so-called *Orr–Sommerfeld* equation (cf. White [42] or Schlichting [36])

$$(U - \omega/\overline{\alpha}) \left(\frac{\partial^2 \tilde{v}}{\partial y^2} - \overline{\alpha}^2 \tilde{v} \right) - \frac{d^2 U}{dy^2} + \frac{i}{\overline{\alpha}\overline{Re}} \left(\frac{\partial^4 \tilde{v}}{\partial y^4} - 2\overline{\alpha}^2 \frac{\partial^2 \tilde{v}}{\partial y^2} + \overline{\alpha}^4 \tilde{v} \right) = 0 \quad . \tag{1}$$

This is based on the assumptions of an incompressible fluid, the so-called parallel-flow approximation (i.e. only wall-parallel flow $U(y)$, no base-flow gradients in x), small disturbance amplitudes and normal disturbance modes of the kind

$$v(x, y, z, t) = \epsilon \, \tilde{v}(y) \, \exp^{i(\alpha x + \gamma z - \omega t)} + c.c. \quad , \tag{2}$$

$$\overline{\alpha} = \sqrt{\alpha^2 + \gamma^2} \qquad \overline{Re} = \frac{\alpha}{\overline{\alpha}} Re \quad , \tag{3}$$

where Re is the Reynolds number, ϵ is an amplitude, $\tilde{v}(y)$ stands for the (complex) disturbance eigenfunction, i is the imaginary unit, α a streamwise wave number, γ a spanwise wave number, ω the circular frequency, and *c.c.* denotes the complex conjugate. The normalized frequency ω of LST is related to the physical frequency f $[Hz]$ via

$$\omega = 2\pi \, f \, L/U_\infty \quad , \tag{4}$$

where L is the reference length in $Re = U_\infty L/\nu$. Two-dimensional disturbances are obtained for $\gamma = 0$ and three-dimensional modes $\gamma \neq 0$ travel in oblique directions with an angle of

$$\psi = atan(\gamma/\alpha) \tag{5}$$

relative to the x-axis.

The solution of equation (1) consists of solving an eigenvalue problem either for $\overline{\alpha}$ or for ω (depending on the choice which of the two is prescribed by the user). Complex $\overline{\alpha}$ means spatial amplification if α_i is negative, and complex ω stands for temporal amplification if $\omega_i > 0$. Different methods to solve the *Orr–Sommerfeld* equation are available (e.g., Alam & Sandham [1], or Allen & Riley [2], Gaster [11], Michalke [25]). Basically a so-called "shooting method" which solves for the most unstable eigenvalue can be constructed or a "matrix method" which computes every eigenvalue of the discretised equation (including the so-called discrete spectrum). We have chosen a discretisation of the y-derivatives using sixth-order accurate finite differences on a fine grid and *EISPACK* routines to solve the eigenvalue problem. The computer codes have been verified by comparisons with results published in literature, DNS and by comparing results of the two methods.

3.0 RESULTS

In the following subsections we present comparisons of DNS results with linear stability theory (LST), several investigations based on LST related to the influence of the wall on the free shear-layer instability and on the possible occurrence of an absolute instability. Then, DNS will show the non-linear influence of the disturbances on the mean flow and we shall compare several mechanisms associated with the question of how can turbulence (which is inherently three-dimensional) arise in a flow that is dominated by two-dimensional instabilities.

3.1 Base Flow

The subsequent examples are all presented for $Re = U_\infty \cdot L/\nu = 100000$, where L is an arbitrary reference length used for normalisation of the coordinates. For a *Blasius* boundary layer the x-coordinate can be converted to the Reynolds number based on the displacement thickness δ^* via $Re^* = 1.72077\ \sqrt{x \cdot Re}$. This is always possible at the inflow boundary of the integration domain because all flows start with the *Blasius* boundary layer at inflow. Further downstream Re^* increases much faster than for the *Blasius* boundary layer due to the displacement effects of the flow with laminar separation bubble.

The streamwise velocity $U_p(x)$ used to create a LSB for the subsequent investigations is compared to many classical boundary layer parameters in Fig. 5. The wall pressure rises in accordance with the Bernoulli equation so that the laminar boundary layer separates near the centre of the adverse pressure gradient region. A constant pressure plateau after separation in $1 - p_w$ is not observed, however. The wall shear becomes negative inside the bubble and asymptotically recovers towards the *Blasius* value downstream of the LSB. The separation streamline of the bubble exhibits a quasi-symmetrical lens-like shape. The displacement thickness δ^* and the shape factor $H = \delta^*/\Theta$ (Θ = momentum thickness) increase considerably around the bubble. Separation and re-attachment occur around $H \approx 3.8 - 3.9$, i.e. at somewhat lower values than for a *Falkner–Skan* boundary layer at separation. Accordingly, the shape parameter δ^{**}/Θ (δ^{**} = energy thickness) at (S) and (R) is also different from $\delta^{**}/\Theta = 1.515$ because the present results are from a full Navier–Stokes simulation and not from a similarity solution.

An illustration of the complete flow field is given in Fig. 6 using streamlines, some characteristic velocity profiles and vorticity contours. The reverse flow in the present bubble is rather small with accordingly small negative vorticity inside it. The vorticity maximum of the boundary layer leaves the wall already well upstream of separation. After re-attachment the vorticity close to the wall becomes rather constant in agreement with Fig. 5 a).

3.2 Primary Instability

Classical linear stability theory (cf. subsection 2.2) considers the instability of a velocity profile with respect to small two- or three-dimensional disturbances. Since this is the first instability in a sequence leading to turbulence, it is also called "primary instability".

Our present knowledge of the primary instability of laminar separation bubbles stems mainly from some theoretical investigations based on hypothetical, free shear-layer like base-flow profiles or modifications thereof [2, 7, 11, 13, 26, 27]. These have the advantage that the influence of parameter variations can be easily studied. But such profiles do not correspond to an actual flow field that fulfils the Navier-Stokes equations. In addition, a local analysis neglects the streamwise structure of the flow (so-called nonparallel effects). However, in direct quantitative comparisons of DNS results with linear stability theory based on base- or mean-flow profiles of the simulations we have already shown that small-amplitude disturbances evolve in an extremely good agreement with linear stability theory despite its approximate manner. This is confirmed in Fig. 7 where

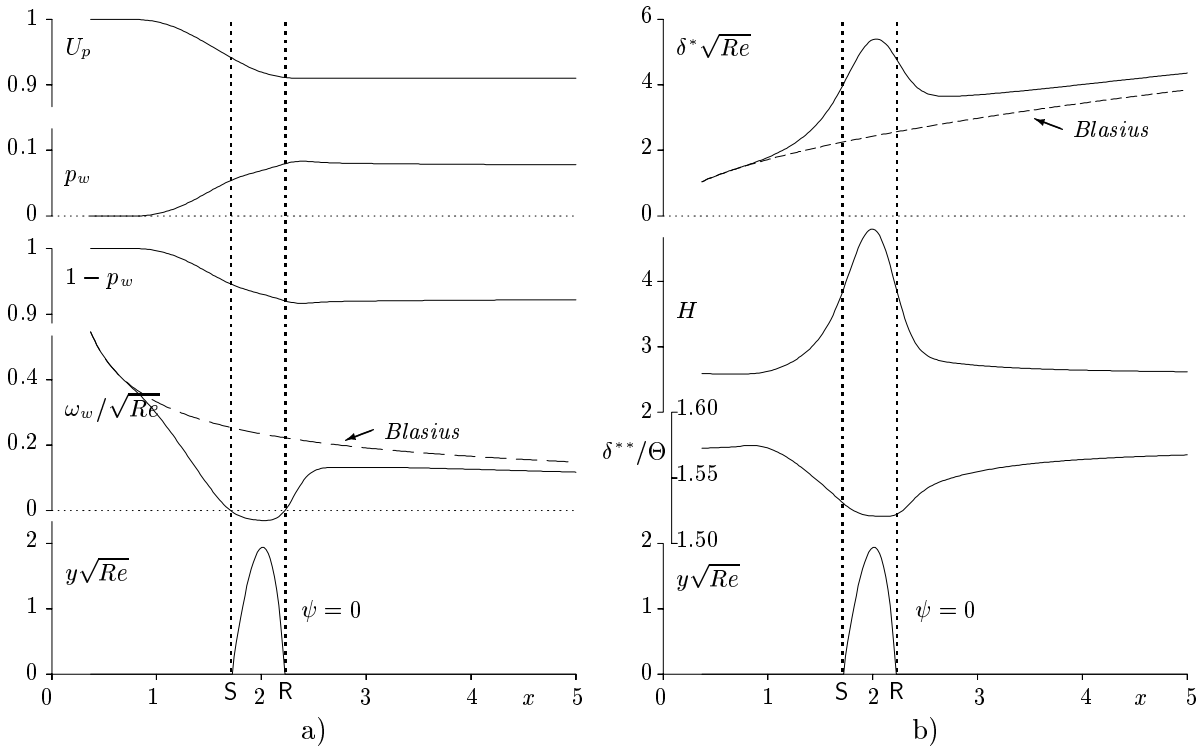

Figure 5: Boundary layer parameters of the steady base flow. a) Velocity U_p at the free-stream boundary, wall pressure p_w, wall friction $\omega_w = \partial U/\partial y|_w$ and separation stream line $\psi = 0$; b) displacement thickness δ^*, shape factors $H = \delta^*/\Theta$ and δ^{**}/Θ; separation streamline $\psi = 0$; (S = separation, R = re-attachment).

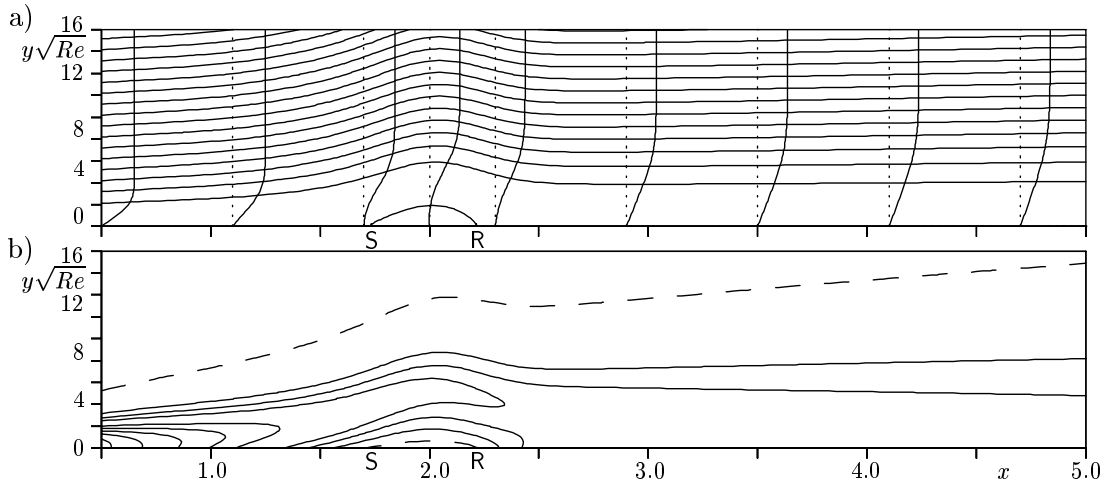

Figure 6: Illustration of the steady base flow. a) streamlines ($\psi = 0, 1, 2, 3, \ldots$) and boundary layer velocity profiles; b) vorticity contours (ω_z = 0,0001, 0,05, 0,10, 0,15, ...; ω_z = 0,0001 dashed).

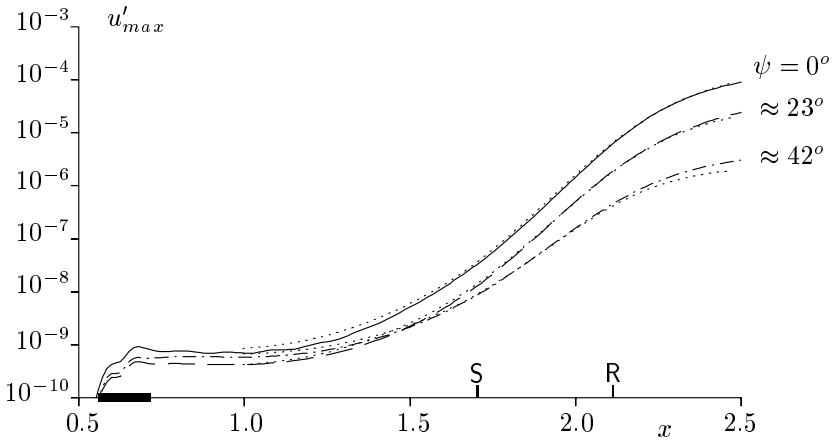

Figure 7: Comparison of u' disturbance maxima with results of linear stability theory ($\cdots$). S = separation; R = re-attachment; ▬ = location of disturbance strip; wave angle $\psi = atan(\gamma/\alpha)$.

the normal-to-the wall maxima of the streamwise velocity fluctuation u' for Tollmien-Schlichting waves with different propagation angle relative to the base flow are displayed. A more complete description of these results can be found in [33] and [35], for instance.

These results also show that the disturbance growth with downstream coordinate x increases in a very gradual way already well upstream of the separation point (S). In consequence, there is no reason to distinguish between a free shear layer or 'Kelvin-Helmholtz' instability and the TS-instability of a boundary layer.

The complete stability diagram (for 2-D disturbances only) of the present LSB is displayed in Fig. 8 in comparison with the one for the *Blasius* boundary layer ($dp/dx = 0$) at inflow. For the bubble a much wider region of unstable frequencies appears together with much larger (about 16-fold) amplification rates in the centre of the bubble. Downstream of the laminar separation bubble the instability returns to that of a *Blasius* boundary layer in accordance with the relaxation of the base flow shown in Fig. 5.

3.3 Influence of the Wall

A quantitative investigation of the influence of the wall on linear stability theory results has been performed [30, 35]. Figure 9 illustrates the findings of that research for two different wall distances of the "free shear layer". The dashed curves correspond to a boundary layer profile taken from the previous example at $x = 2.0$, where the separation bubble exhibits the strongest reverse flow. This profile was then modified, first by a small shift in u-direction by the amount of maximal reverse flow in order to make that zero [curve (1)], then by different shifts away from the wall, padded with zero velocity [curve (2)]. In any case, a viscid investigation was performed for finite Reynolds number. The results for the largest wall distance in Fig. 9 b) and d) agree extremely well with the spatial instability of an inviscid shear layer, the so-called "Kelvin–Helmholtz" instability, cf. [25, Fig. 2]). However, for small frequencies, there is an influence of the wall that can be seen in the difference of the phase speed from the theoretical value of 1 in Fig. 9 c). Thus, the instability and the eigenfunctions of the profile extracted from the DNS-bubble are really far away from an inviscid free shear-layer instability. They belong to the "Tollmien–Schlichting" instability, which is of viscid nature (because it vanishes at $Re \to \infty$).

As already shown above, the shift-over from TS- to KH-instability is a very smooth process. This leads to an accordingly smooth evolution of the eigenfunctions of the disturbances: for

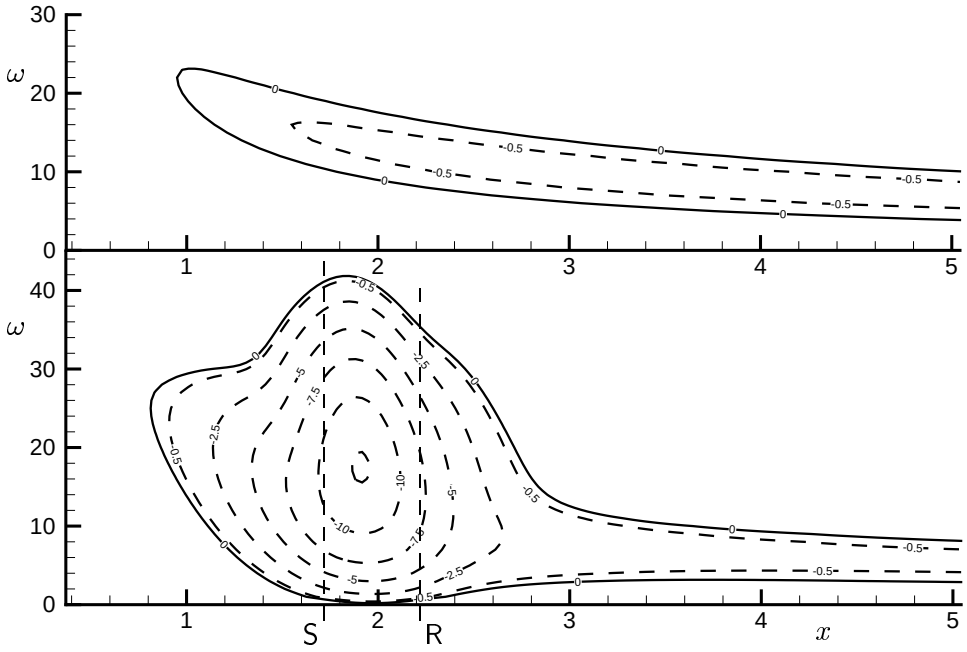

Figure 8: Stability diagrams for the *Blasius* boundary layer (top) and for the LSB in Figs. 5 and 6 (bottom). S = separation; R = re-attachment.

a TS-wave the disturbance maximum is close to the wall followed by a phase jump, a second maximum, and exponential decay further away, while for a KH-mode there is a maximum exactly at the inflection point of the base-flow profile followed by a sharp phase jump towards the low speed side of the flow and exponential decay in both directions after a certain distance from the high-shear region. Therefore, the profiles in the changeover region which are characteristic for LSBs have three distinct maxima. For practical purposes their relative magnitude can be used to assess the amount of contribution of the KH-instability to the TS-instability: a large shear-layer maximum would indicate more contribution of the shear-layer instability, and vice versa. Since the wall distance of the separated shear layer in a pressure-induced laminar separation bubble (in contrast to a laminar separation bubble behind a step) increases steadily the initial instability is of TS-type in any case. In conclusion of this little exercise, one may say that a contribution from a KH-instability can be expected only for accordingly large shear-layer distances from the wall (i.e., in the rear part of the bubble close to transition, or for LSBs behind steps).

3.4 Absolute vs. Convective Instability

A long-standing question among many researchers has been the issue whether transition in a laminar separation bubble occurs due to an absolute instability of the flow. The concepts of absolute and convective instability are decisive for a number of reasons. Let us therefore first look at the basic ideas and at their consequences for flow prediction and control, and then address the question of finding conditions for their occurrence in a laminar separation bubble. An introduction to the concepts of absolute and convective instabilities can be found in Huerre & Monkewitz (1985) [15], for instance, from which the present figure 10 is adopted. This figure sketches the spatio-temporal evolution of a small pulse-like disturbance in a laminar flow. If the disturbance is swept away from the source while it amplifies as in Fig. 10 a), one speaks of a *"convective instability"*. One characteristic feature of this is that the flow will return to its initial undisturbed state when the wave packet has moved by or when the forcing is stopped. Another feature of this situation is that the local flow (i.e. for a certain x) will depend on what happened upstream. Thus, the boundary layer merely acts as a disturbance amplifier. In consequence of this a convectively unstable flow is controllable.

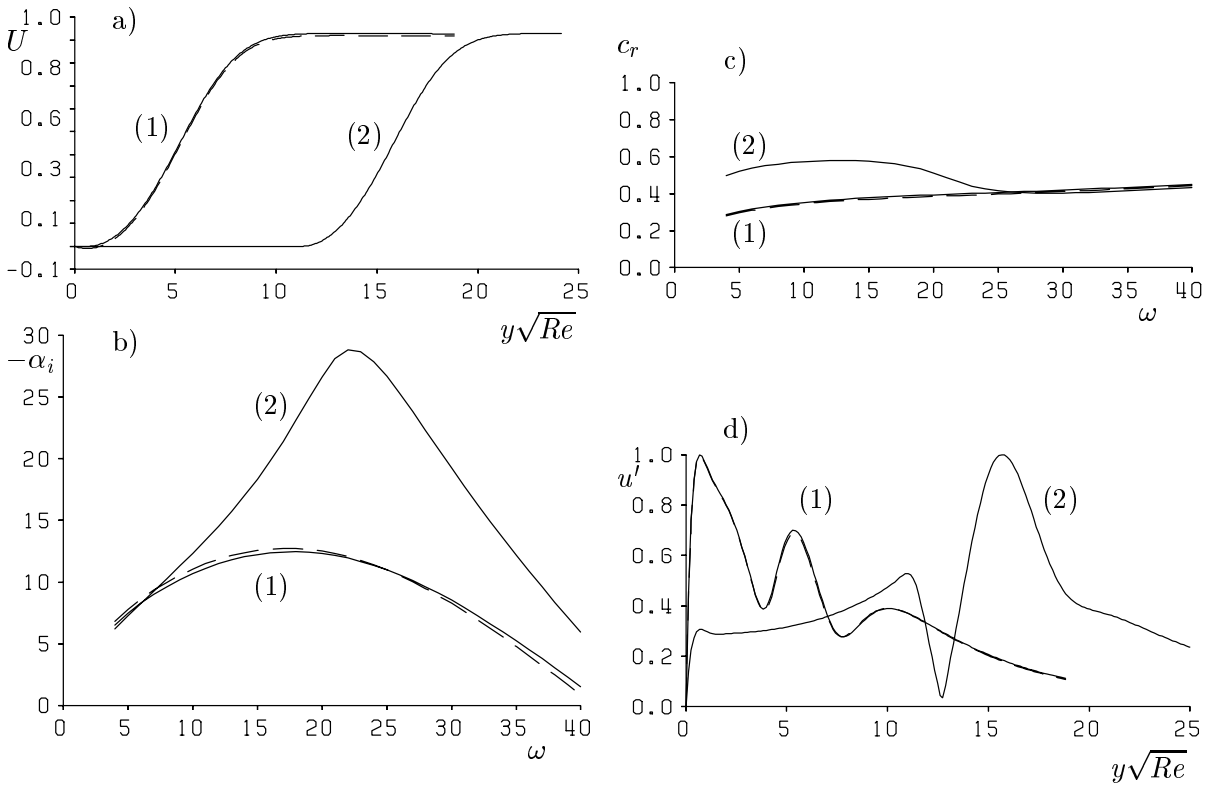

Figure 9: Investigations on the influence of the wall on the instability of the separated shear layer. a) base flow. Dashed line: profile extracted at $x = 2$ from the LSB in Fig. 6; (1) = profile shifted to remove reverse flow at the wall; (2) = profile after a large shift away from the wall. $Re = 100000$. b) amplification rates; c) phase velocities; d) eigenfunctions for $\omega = 20$.

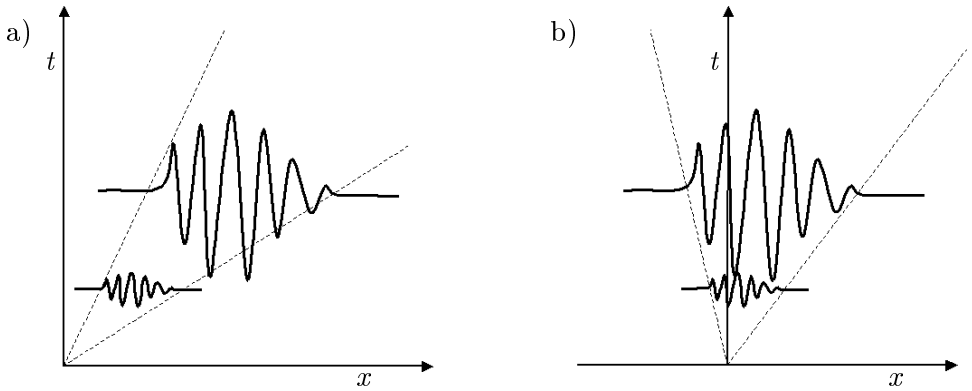

Figure 10: Basic concept for convective (a) and absolute (b) instability after Huerre & Monkewitz (1985) [15]

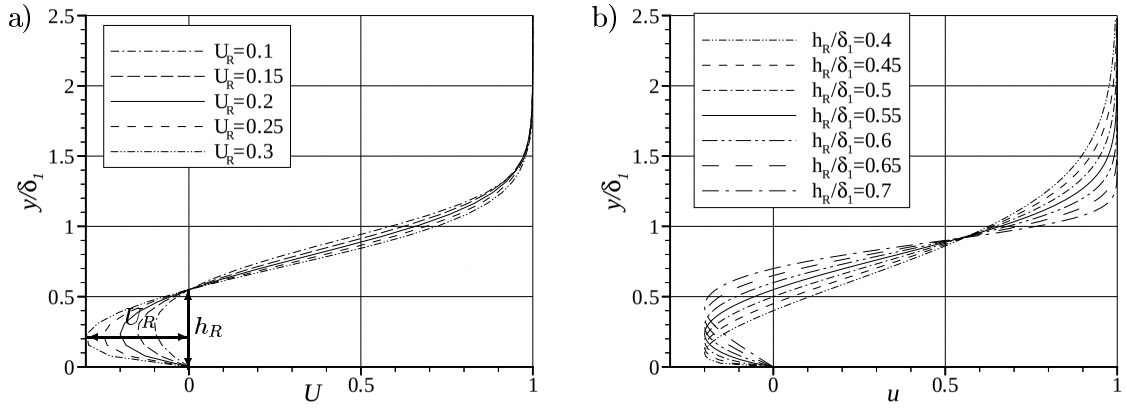

Figure 11: Examples of analytical velocity profiles. a) Variation of the reverse-flow intensity U_R for constant height $h_R/\delta^* = 0.55$ of the reverse flow zone; b) variation of the height for constant reverse flow $U_R = 0.2$.

In the case of an "absolute instability" in Fig. 10 b) one observes a local growth of the disturbance amplitude for $x = const$ because the wave packet spreads more rapidly than it is convected away. It is important to note that an absolute instability cannot be stopped once initiated. The flow will unavoidably turn to a different state. Thus, it is no longer dependent on the upstream disturbance spectrum and it cannot be controlled by intentional upstream forcing.

Therefore, it is important to know which of the two concepts applies for a particular laminar separation bubble. This question has a long history, but in recent years the situation has been considerably clarified by several investigations using linear stability theory (e.g., Michalke [26], Gaster [11], Allen & Riley [2], Hammond & Redekopp [13], Alam & Sandham [1], Rist & Maucher [34], and others). A common basis for such investigations is the assumption of a class of boundary-layer profiles which are controlled by few parameters. According profiles of Maucher [20] are shown in Fig. 11. They are characterized by three parameters: the reverse flow velocity U_R, some Reynolds number, and some measure for the distance of the shear layer from the wall, i.e., the height of the reverse-flow region h_R. For the Reynolds number we use Re^* which is based on the displacement thickness δ^* of the profile. Other length scales or the maximum shear of the profiles could have been taken equally well, but the present results can be easily recast with respect to such base-flow parameters.

Increasing the reverse-flow intensity U_R leads to a gradually larger reverse-shear layer at the wall because of the no-slip condition, while the maximum shear in the detached shear layer is only slightly increased (Fig. 11 a). Therefore, the main influence of the reverse flow on the linear flow instability is through the differences near the wall which are of viscous nature and hence Reynolds number dependent. On the other hand, larger wall distances increase the shear layer maximum and decrease the wall shear so that the instability of such profiles will be dominated by free shear layer effects, which are of inviscid nature.

Due to the normalisation of the profiles with respect to each profile's displacement thickness, the maximum shear of the profiles increases with increasing height h_R. Regardless of how the analytical profiles were constructed these two parameters would always be connected with each other. Using our normalisation a change in Reynolds number does not modify the base flow profiles.

To find the border between convective and absolute instability the wave number α and the frequency ω in equation (1) must be both treated as complex numbers and the streamwise group

velocity

$$c_g = \partial\omega/\partial\alpha \tag{6}$$

must be considered. According to Gaster [10] the possibility of a true time-growing instability needs modes with zero group velocity, because then the energy is not convected away from the source anymore. For the present investigations this means

$$c_g = 0 \quad \text{and} \quad \omega_i > 0\,. \tag{7}$$

The *Orr–Sommerfeld* solver described in subsection 2.2 has been adapted for the present investigations. Starting from a known eigenvalue (or close to it) the 4-D space which is spanned by α_r, α_i, ω_r, and ω_i is investigated for a certain base-flow profile $U(y)$ and Reynolds number Re^*. Once a few eigenvalues are known, the group velocity can be easily computed by (finite-difference) differentiation of the eigenvalues. The code then automatically searches for the eigenvalues with zero group velocity. As already shown above, the mean-flow profiles are characterized by the height of the reverse flow region h_R and its intensity U_R.

From the work of Gaster (1991) [11] it is known that a reverse-flow profile with $U_R = 14.5\%$ is at the edge of absolute instability. His results have been compared with the present research in Rist & Maucher (2002) [34], and a good agreement has been found.

All present results for $U_R = 0.20$ and various reverse flow heights h_R are shown in Fig. 12[2]. Apparently, the influence of the Reynolds number on the eigenvalues is confined to $Re^* < 5000$ and $h_R < 0.5\,\delta^*$ which means that a large portion of the instability is inviscid. Generally, larger wall distances lead to smaller streamwise scales (i.e., larger wave number α_r), higher frequency ω_r, as well as larger spatial and temporal amplification. Note that all eigenvalues shown exhibit rather large spatial downstream growth because $\alpha_i < 0$. However, a time-growing instability ($\omega_i > 0$) can only be expected for the two profiles with the largest wall distance of the shear layer (i.e., $h_R/\delta^* = 0.65$ and 0.70) despite the fact that $U_R = 0.2$ is larger than the limit $U_R = 0.145$ for absolute instability found by Gaster [11]. Since the maximum shear in the corresponding base-flow profiles is largest, this could also be understood as an effect of increasing shear-layer strength. In any case, the present results demonstrate that more parameters than the maximum reverse flow strength and Reynolds number must be considered to adequately describe the problem. The complete set of diagrams for other reverse-flow intensities can be found in Maucher (2001) [20].
From the investigations which have been performed in the region

$$400 \le Re^* \le 25000\,, \quad 0.1 \le U_R \le 0.3\,, \quad 0.4 \le h_R/\delta^* \le 0.7 \tag{8}$$

it appears that the general effect of reducing the reverse flow is to decrease α_r and α_i, to increase the frequency ω_r and to reduce the temporal amplification rate ω_i. Increasing the back flow has the contrary effect. Figure 13 summarizes these effects with respect to the temporal amplification rate, where $\omega_{0,i}$ denotes temporal amplification rates of eigenvalues with zero group velocity. Growth occurs for $\omega_{0,i} > 0$, i.e., above the surface $\omega_{0,i} = 0$. The reverse-flow intensity increases from front to back and its thickness from bottom to top.

The present results indicate that time-growing disturbances can be met not only when the intensity of reverse flow is increased beyond 15% but also when the thickness of the reverse-flow zone exceeds $h_R/\delta^* = 0.5$. A weak Reynolds number influence is also observed. From Fig. 13 it is clear that the most unstable modes with $\omega_i > 0$ must be expected in the corner where all three parameters are largest, and that reducing every one of the three reduces time-growing instability. Meanwhile, the above theoretical predictions have been validated by comparisons with two DNS, one in [34], the other unpublished.

[2] double indices $(0, r/i)$ are used to remind the reader that only modes with $c_g = 0$ are considered

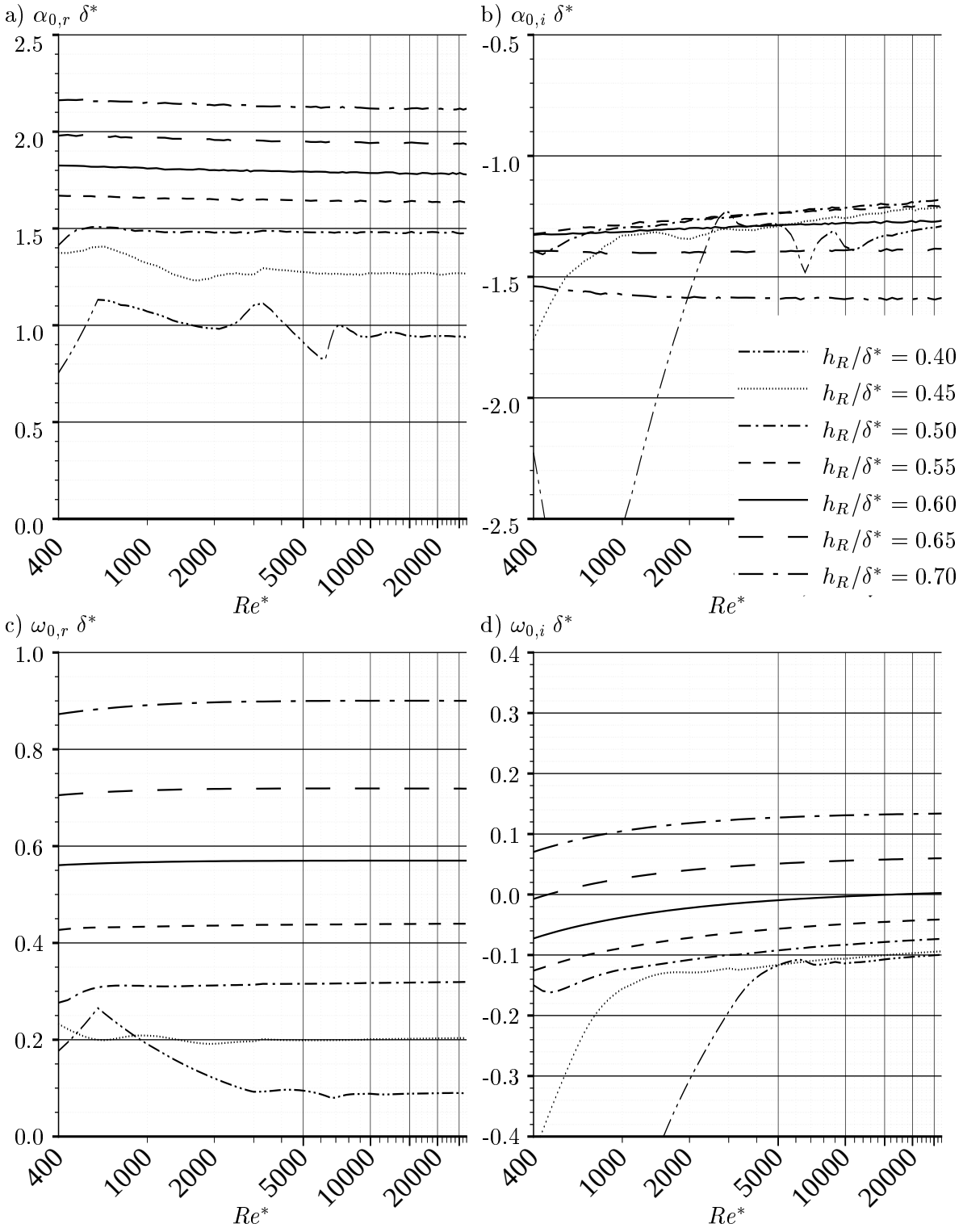

Figure 12: Eigenvalues with zero group velocity for $U_R = 0.20$; a) $\alpha_{0,r}$, b) $\alpha_{0,i}$, c) $\omega_{0,r}$, d) $\omega_{0,i}$

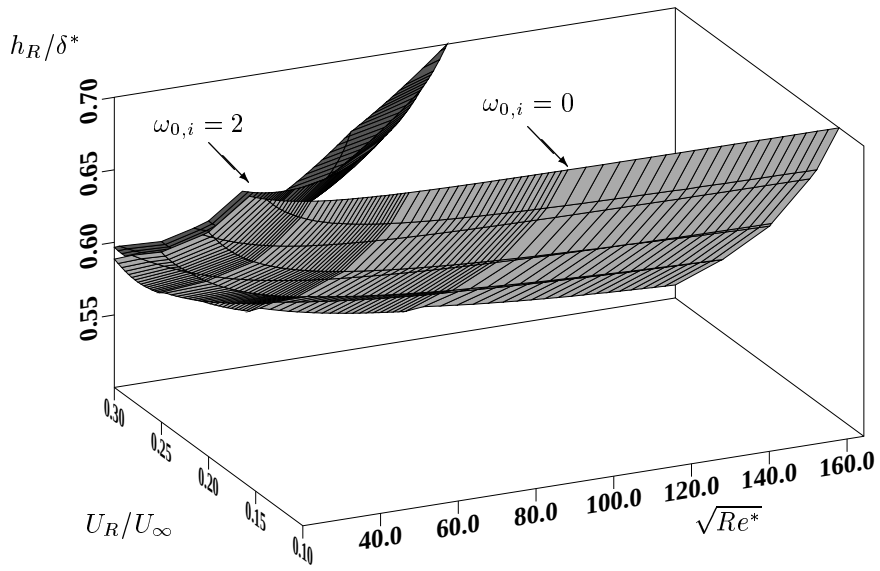

Figure 13: Iso-surfaces of constant temporal amplification.

3.5 Influence of Disturbance Amplitude on Bubble Size

In a LSB instability and base flow are coupled much closer than in an attached boundary layer. Due to large amplification rates and various instabilities, disturbances can reach a non-linear regime within the bubble even if their initial amplitude is 'negligibly' small. Once they are large enough they impose changes on the mean flow in a non-linear manner (that is difficult to predict). Changes of the mean flow can alter the instability and hence the growth of disturbances that follow. An example for such a case where the laminar separation bubble exhibits a low-frequency change of its stability characteristics is described in [20] and [34].

Now we consider a simulation with larger Re^* at inflow and hence larger Re^* at separation (1722 and 2700, respectively), because the observed effect is more pronounced for larger Re^*. Upstream forcing is applied with $\omega = 5$ and three different disturbance amplitudes for the wall-normal velocity component are used: 10^{-4}, 10^{-5}, and 10^{-6}, respectively. The according maxima of the streamwise velocity disturbance u' are shown in Fig. 14 and the points of non-linear saturation of each case are marked by three arrows that touch the respective curve. The results are as expected: For larger forcing transition (in the present simulations, the point of non-linear saturation of the disturbances) occurs further upstream than for small disturbance amplitudes. Since earlier transition means earlier re-attachment, it can be expected that the bubble becomes shorter from its rearward end, a fact that is actually observed in the streamline plots of Fig. 15. However, this is not the only effect of the disturbances, since the separation point moves downstream an equally large distance at the same time. A further remarkable effect is that the mean-flow profiles (Fig. 16) exhibit a rather unexpected strong dependence on the disturbance amplitudes, as well. Thus, the difference between two profiles is orders of magnitude larger than the local disturbance amplitude (compare Fig. 14 and Fig. 16). A very similar effect has also been discovered in wind-tunnel experiments by Dovgal *et al.* [7].

Further analysis of the DNS data has shown that this coupling of transition, re-attachment, and separation is related to subtle changes in the streamwise pressure gradient along the wall. In a pressure-induced separation bubble, (S) is not fixed by some surface irregularity and hence highly sensitive to small changes in pressure. Thus, it turns out that a pressure-induced LSB is very sensitive to background disturbances and that these should be taken into account when comparing simulation results with experiments.

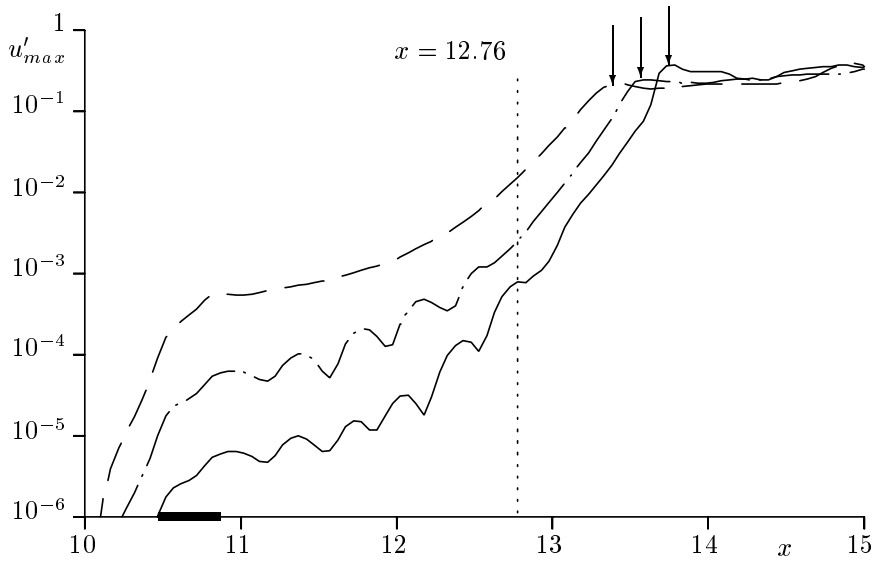

Figure 14: Comparison of disturbance amplitudes for different forcing at the wall: $A_v = 10^{-4}, 10^{-5}, 10^{-6}$ (top to bottom). Arrows point to the position of non-linear saturation (e.g. transition); ▬ = location of disturbance strip.

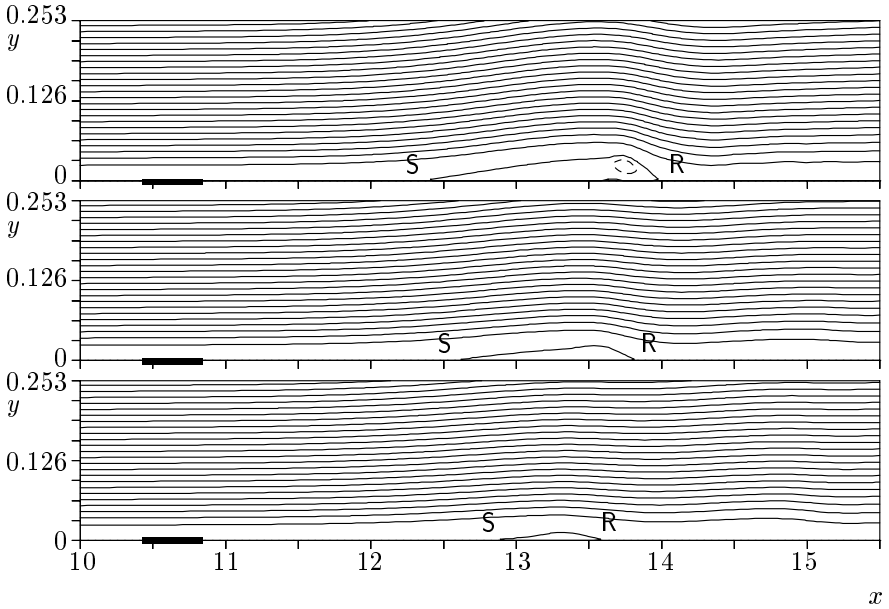

Figure 15: Mean-flow streamlines for simulations with three different forcing amplitudes: $A_v = 10^{-6}, 10^{-5}, 10^{-4}$ (from top to bottom). S = separation; R = re-attachment; ▬ = location of disturbance strip.

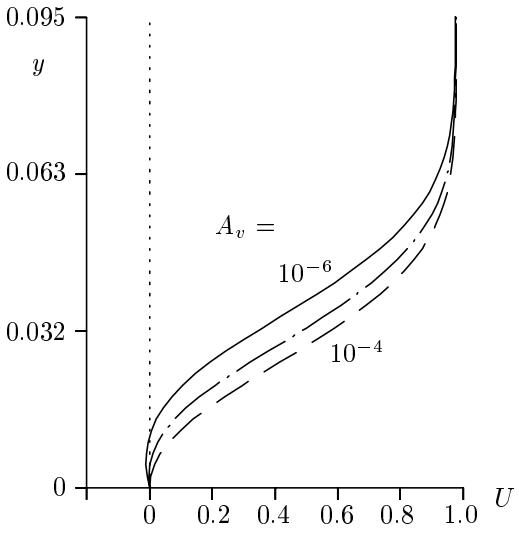

Figure 16: Comparison of mean-flow profiles at $x = 12.76$ for different forcing at the wall.

3.6 Secondary Instability

In a two-dimensional boundary layer, three-dimensional disturbances become strongly amplified by a parametric resonance once two-dimensional primary disturbances have attained sufficiently large amplitudes [14]. Characteristically, this kind of secondary instability amplifies disturbances with subharmonic or fundamental frequency with respect to the two-dimensional one, and its amplification rates are typically one order of magnitude larger than that provided by primary instability. Due to non-linear interactions the wavenumber-frequency spectrum fills up very rapidly which indicates a breakdown of the flow into small-scale unsteady structures. For many laminar separation bubbles, however, our simulations show that such an instability is only marginally relevant because it is restricted to a very narrow streamwise region. Two typical results are illustrated in Figs. 17 through 19 for subharmonic and fundamental secondary instability, respectively. More information can be found in [30, 33, 35].

In Fig. 17 the fundamental ($\omega = 18$) two-dimensional disturbance is forced at $x \approx 0.65$ together with a pair of subharmonic ($\omega = 9$) three-dimensional disturbances at small amplitude ($u'_{max} \approx 10^{-9}$ in contrast to $u'_{max} \approx 10^{-4}$ for the fundamental). For comparison, results of primary instability (LST) and of secondary instability theory (SST) [14] are also included (with their initial amplitudes adjusted to the DNS). Due to the presence of the laminar separation bubble, the amplification rate for the primary instability is now one order of magnitude larger than in a *Blasius* boundary layer and an additional amplification of 3-D disturbances due to secondary instability that starts around $x = 1.8$ as the 2-D disturbance passes 1% is not as dramatic as might be expected. In addition, once the 2-D disturbance saturates at $u' \approx 20\%$ the secondary amplification is greatly reduced such that, for the present choice of initial amplitudes, the 3-D disturbances do not reach a saturation level within the integration domain.

Flow visualisations have shown that the 3-D disturbances of the SST get destroyed by the 2-D ones in the saturated regime, see Fig. 18. 3-D vorticity is redistributed and convected away by the large-amplitude 2-D rollers that develop downstream of the bubble. The higher harmonic wave components which are also included in Fig. 17 confirm this process by their large amplitudes. In fact, large-amplitude 2-D forcing can control the flow by delaying transition, a detail that has independently been observed in experiments by Dovgal et al., for instance.

At this point, a subharmonic scenario (that would lead to so-called H-type transition in a

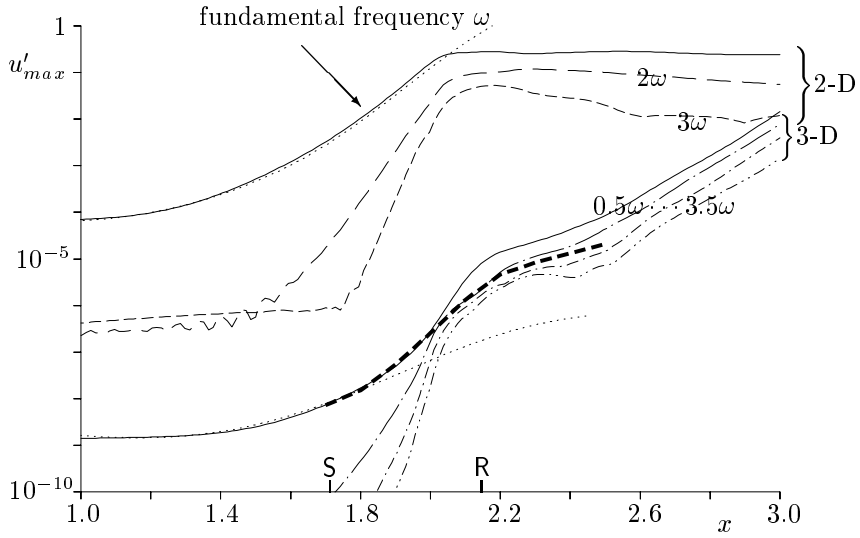

Figure 17: Amplification curves u'_{max} of two- and three-dimensional disturbance components for the case with subharmonic resonance. Comparison with LST ($\cdots$) and SST (- - -). S = separation; R = re-attachment.

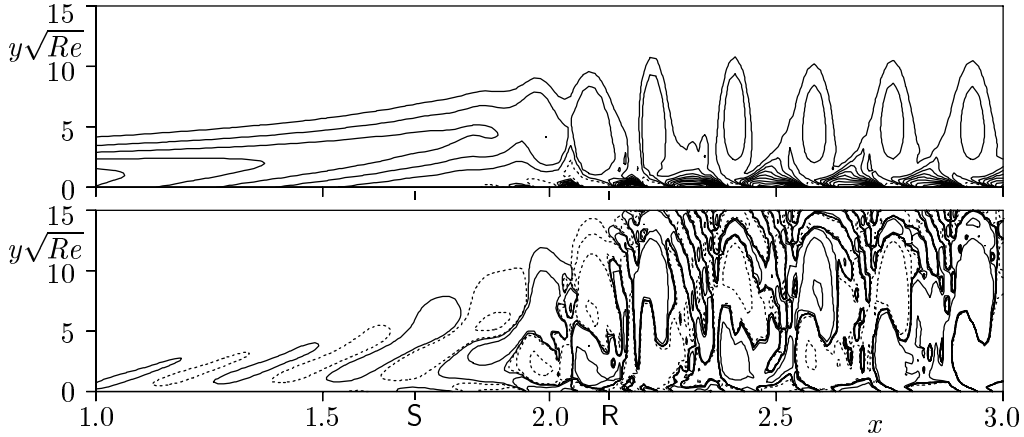

Figure 18: Comparison of instantaneous 2-D vorticity (top) with instantaneous 3-D disturbance vorticity (bottom); dashed lines = negative vorticity

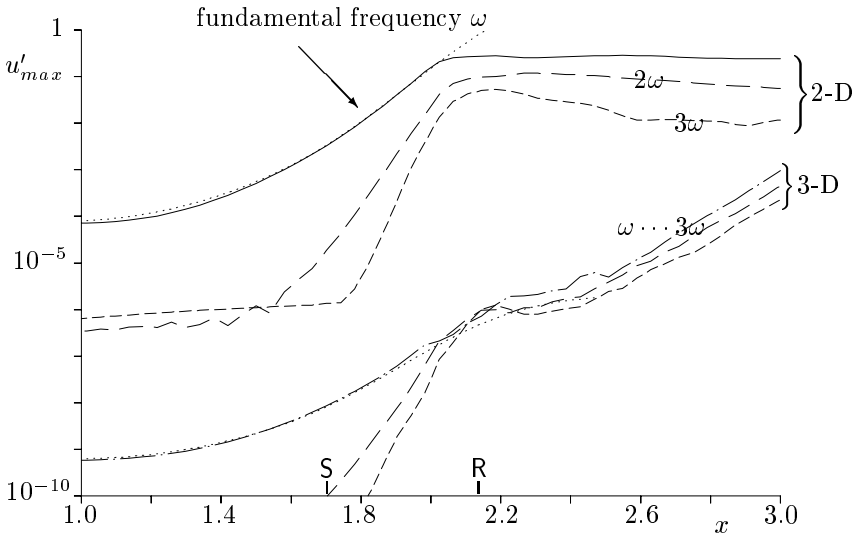

Figure 19: Amplification curves u'_{max} of two- and three-dimensional disturbance components for fundamental resonance. Comparison with LST ($\cdots$). S = separation; R = re-attachment.

Blasius boundary layer) has been studied. An according investigation for fundamental resonance (K-type) is discussed next in connection with Fig. 19. Mixed scenarios, for the base flow considered here, as well as for the one presented in Fig. 15 have been investigated as well, they can be found in [30, 33, 35].

The two-dimensional disturbance development for the *fundamental* scenario is the same as that in the *subharmonic* one, because the three-dimensional disturbance level is kept so low that no non-linear reaction of the 3-D on the 2-D modes occurs. The initial three-dimensional disturbance (dash-dotted line in Fig. 19) results from an interaction of the 2-D fundamental with a steady 3-D disturbance at the disturbance strip (upstream of $x = 1.0$). In consequence, only integer multiples of the fundamental frequency ω appear now for the 3-D modes. Both fundamental waves (2-D as well as the 3-D) amplify according to LST until transition. In contrast to the subharmonic case there is no additional amplification due to secondary instability. Here, the 3-D disturbances are picked up at non-linear saturation of the 2-D wave, as in the previous case shown in Fig. 18. Because of this failure of the secondary instability mechanism to bring arbitrarily small 3-D disturbances directly to non-linear saturation, an alternative has been searched for. This is shown in the next subsection.

3.7 Oblique Breakdown

As an alternative to classical secondary instability scenarios, a mechanism which was first discovered for transonic flow and termed "oblique transition", because of its dependence on the non-linear interaction of oblique waves, was investigated as well [29].

Figure 20 depicts the evolution of the spectral amplitudes of this case in the same base flow as before. Here, the first index for a frequency-spanwise-wavenumber mode means multiples of the fundamental frequency and the second multiples of the basic spanwise wavenumber $\gamma = 2\pi/\lambda_z$. Now, the primary disturbance (identified as mode (1, $\pm$1) consists of a pair of oblique Tollmien-Schlichting waves ($\omega = 18$) with an initial angle of $\psi \approx 28^o$ relative to the x-axis and an initial amplitude $u'_{max} \approx 10^{-4}$. Clearly, the dominant mode follows linear stability theory rather closely. All other modes arise due to non-linearity which leads to a rapid fill-up of the spectrum at $x \approx 2.0$. Since the largest of the non-linearly generated modes is mode (0,2) the re-

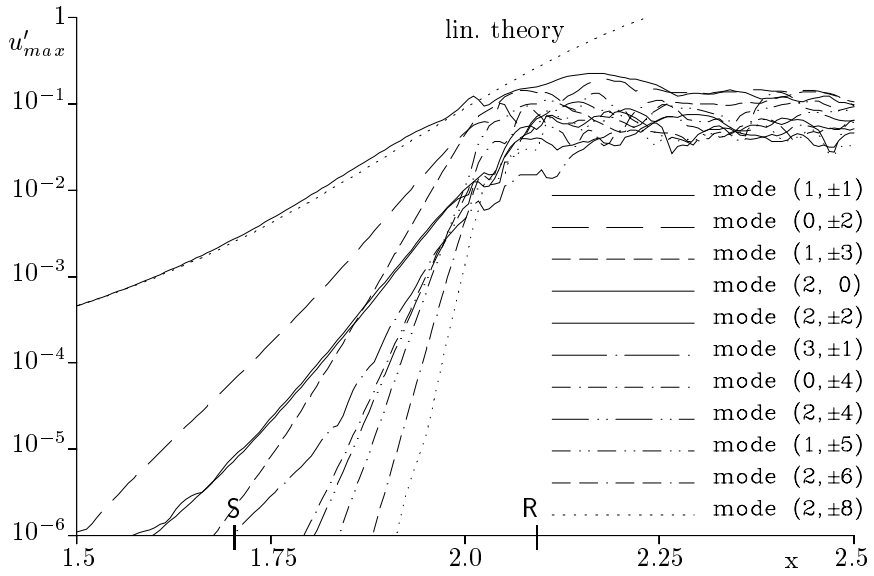

Figure 20: Amplification of individual spectral modes for large 3-D disturbance amplitude.

attachment, as well as the ensuing boundary layer, exhibit longitudinal streaks in the temporal mean. Occasionally, such streaks have already been observed in experiments, e.g. [3]. Inger has tried to relate them to a Görtler instability [16]. However, for the present case it is clear that they arise from transition, since they are an inherent property of the so-called "oblique breakdown" scenario.

Further studies of this kind of mechanism showed that the optimal growth of the streak modes appears when oblique waves with an obliqueness angle of $\psi \approx 20^o$ are forced. This occurs because the growth of the primary modes due to LST is reduced for larger angles and because no oblique breakdown is possible for $\psi \to 0$.

A direct comparison of instantaneous vorticity contours from the (hindered) subharmonic scenario in Fig. 17 with those belonging to Fig. 20 is shown in Fig. 21. This illustrates the interpretation given above, that the flow is controlled by spanwise oriented 'rollers' in the first case, and that a rapid breakdown into small-scale structures appears in the second. Such small-scale 3-D structures are necessary for the rapid development of a turbulent boundary layer in a laminar separation bubble. Thus, it appears that the mechanism studied here can be relevant for production of turbulence in a LSB. This has also been verified in mixed secondary-oblique scenarios in [33].

3.8 A New Type of Instability

When the Reynolds number at separation is increased, a hitherto unknown kind of secondary instability mechanism is observed which leads to *temporal* amplification of small-scale three-dimensional disturbances that are trapped in the separation bubble. More information on this case can be found in [20] and [22]. In contrast to above Re^* at separation is now approx. 2400 instead of 1250.

Figure 22 displays amplitudes of selected modes from a fundamental resonance scenario for two time intervals. A large-amplitude 2-D TS-wave has been forced at $x \approx 8$ together with very small 3-D disturbances. Since the 2-D disturbances are periodic they do not differ for a later time compared to the earlier one. This is in clear contrast to the 3-D disturbances which are two orders of magnitude larger for the second time interval shown in the figure. The arrow $\Uparrow$

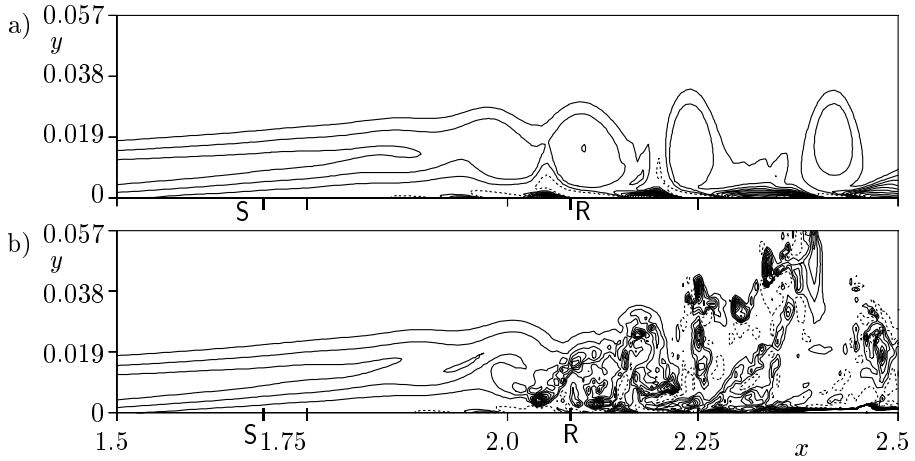

Figure 21: Comparison of instantaneous vorticity contours for subharmonic resonance (a) and "oblique breakdown" (b).

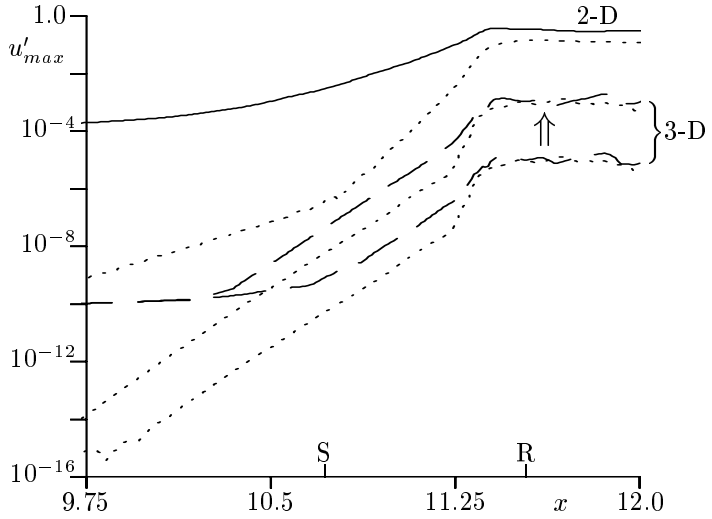

Figure 22: Disturbance amplitudes of 2-D (solid) and 3-D (dashed) waves in the vicinity of the bubble. Dotted lines: higher harmonics; arrow: 3-D temporal growth; S - separation, R - re-attachment.

points to the temporal growth present in the curves for the 3-D disturbances at different time.

It turned out that permanent forcing of the 3-D disturbances is not necessary because a one-instant 3-D time impulse at the wall is sufficient to initiate their growth. A quantification of the temporal growth initiated by a short-time pulse leads to the results presented in Fig. 23, where the dependence of the temporal growth rate ω_i on the spanwise wave number is shown. Alternating regions of subharmonic and fundamental disturbance amplification appear, which indicates that the mechanism found is related to the secondary instability discovered by Herbert [14]. The main difference is their temporal growth in the sense of an 'absolute' secondary instability and their alternating occurrence with increasing spanwise wavenumber.

More investigations with an additional buffer domain applied in the upstream part of the integration domain which affected the 3-D modes only indicated that the responsible area for their amplification is the re-attachment region. By comparing the development of the 3-D disturbances with the dynamics of the 2-D high-shear layer Maucher *et al.* [20, 21, 22] identified the reason for the instability as the entrainment of three-dimensionality by the upstream motion

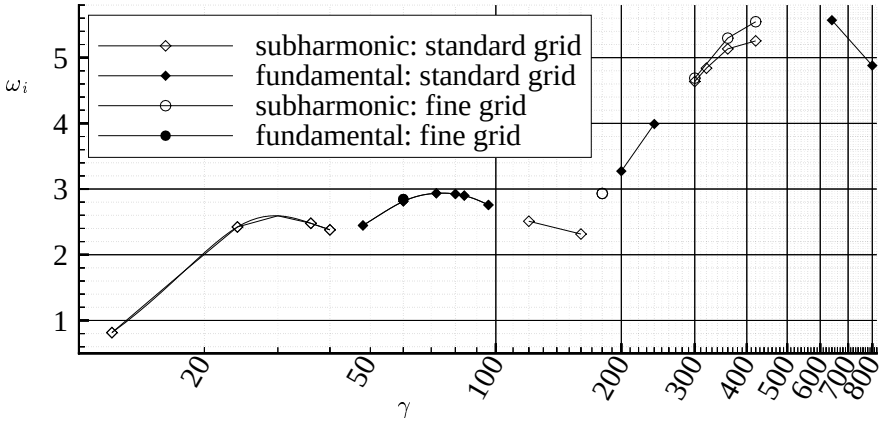

Figure 23: Secondary temporal amplification rate ω_i versus spanwise wave number $\gamma = 2\pi/\lambda_z$ for different discretisations.

in the laminar separation bubble that includes an uplift of 3-D motion into the initially two-dimensional shear layer. Since this process is repeated periodically, the 3-D amplitudes can grow from cycle to cycle until they reach a level with non-linear saturation. Once this level is reached, the process just described is still operative in order to destroy the 2-D shear layer repeatedly. This is visualised by iso-surfaces of spanwise vorticity in Fig. 24. The dynamics of this kind of laminar separation bubble transition resembles the breaking of waves which approach a shore line. An interesting aspect of the scenario shown is that it is very efficient for small obliqueness angles of the involved primary disturbances, i.e. it is not restricted to a strictly two-dimensional disturbance. The lower picture in Fig. 24 shows this for the transition process triggered by a pair of weakly oblique waves [20]. Interestingly, weakly oblique disturbances have been already observed to dominate in several free-flight measurements of the natural disturbance spectra in airfoil boundary layers. Another fact that should be mentioned is that structures which are very similar to those observed in Fig. 24 have been found in hydrogen-bubble visualisations in our water channel, Lang *et al.* (2002) [19]. Thus, it can be expected that the present effect takes place in several real-life applications.

4.0 ADDITIONAL EFFECTS

It appears that many effects are interwoven in an LSB, see Fig. 3 and we have so far only considered instability, non-linear interactions and feedback. Therefore, the so-called 'receptivity', i.e. the generation of initial disturbances, will be addressed in the next subsection. Apart from the unsteadiness that appears due to instability and transition a low frequency phenomenon called 'flapping' may occur in a laminar separation bubble, this will be touched in subsection 4.2. The rather old question of "bubble bursting" (cf. Gaster, 1966 [9]) which is important for airfoil design, is visited in light of the present findings in subsection 4.3.

So far, the effects of an unsteady free-stream flow which is relevant for turbo machines or flapping wings are not yet equally well investigated and understood. Hence they are not considered here. However, the issue of unsteady flow control is directly related to the previous sections. It will be covered in an extra article of this lecture series [31].

4.1 Receptivity

With our finding that most pressure-induced laminar separation bubbles are governed by a convective primary instability, initial disturbances are responsible for the transition process

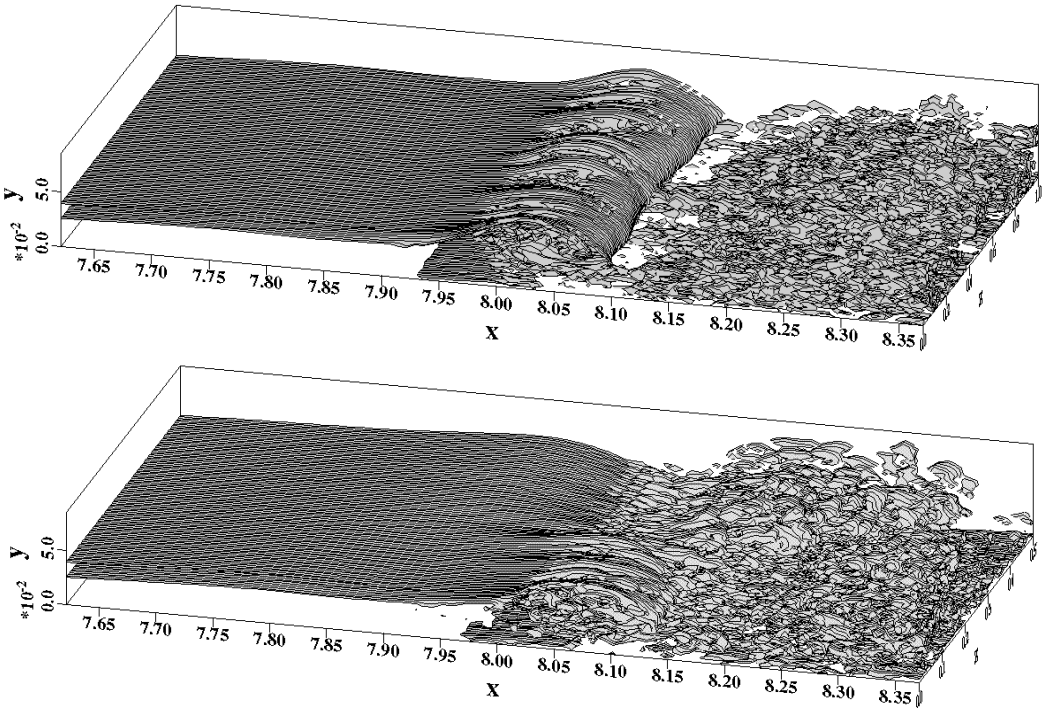

Figure 24: Breakdown of the shear layer at the end of an LSB into fine-scale turbulence. Isosurfaces of the spanwise vorticity. Top: 2-D primary disturbance, bottom: oblique primary disturbance. Note: The coordinates in this figure should be multiplied by 1.5 in order to make the normalisation consistent with the other figures.

and hence for overall features of the bubble. This raises the question of where and how these disturbances are generated. In (incompressible) receptivity theory it is usual to assume two kinds of free-stream disturbances: sound and vorticity. The first has a very high speed compared to the free-stream velocity and hence a large wave length (infinity in the truly incompressible limit), the second has finite wave lengths but it travels at free-stream speed. It appears that a transformation into Tollmien-Schlichting-like boundary-layer waves is only possible in connection with large-enough streamwise gradients in the boundary layer. Such gradients appear at the leading edge of an airfoil and due to surface roughness, which may be distributed or local. Since a laminar separation bubble displaces the flow like a roughness element, one might think that a LSB is a direct source of increased receptivity. Experimental investigations of this hypothesis can be found in Dovgal's work [4, 7].

Here we investigate the problem with theoretical tools. Our discussion is restricted to two-dimensional acoustical perturbations of the free stream because these produce larger disturbances inside the boundary layer than vorticity fluctuations. In linear receptivity theory (based on the *Orr–Sommerfeld* equation or on asymptotic expansions) the source of receptivity can be attributed to a modified wall boundary condition which considers the local interaction of sound and wall roughness

$$u'(y=0) = H(x)\left.\frac{dU}{dy}\right|_{y=0} \quad , \tag{9}$$

where $H(x)$ describes the shape of the roughness and dU/dy is the velocity gradient of the boundary layer at the wall (e.g., Crouch, 1992 [6] or Choudhari, 1993 [5]). From eqn. (9) it follows that receptivity is directly proportional to the wall shear, at least in the linear limit of small disturbances and small roughness heights. A large wall shear occurs in flows with a

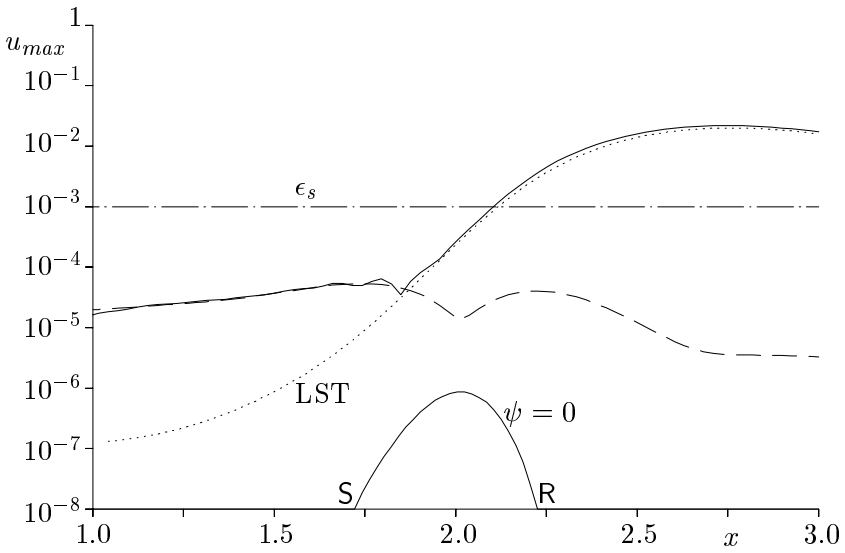

Figure 25: Comparison of maxima of the non-linear forcing term (– – –), linear stability theory (LST) and resulting disturbance (——) for an oscillating free stream ($\omega = 18$, $\epsilon_s = 10^{-3}$).

favourable pressure gradient but these are highly stable with respect to LST. Thus it turns out that receptivity and instability act in an opposite direction to each other such that we must expect reduced receptivity in the highly unstable LSB, instead of the contrary.

This reasoning is in line with the mentioned experiments of Dovgal *et al.* who state that the instability waves found in the bubble originate in the pressure minimum of their airfoil boundary layer, i.e., where the velocity and hence the wall shear are largest. If one considers higher order or more non-linear mechanisms, however, streamwise base-flow gradients should not be neglected.

Figure 25 presents the outcome of an investigation by Stemmer (1995) [30, 37] where the receptivity of the bubble from subsection 3.1 with respect to periodical oscillations of the free stream velocity has been investigated using the complete Navier–Stokes equations in DNS. These oscillations model a 2-D sound wave with circular frequency $\omega_s = 18$, i.e. the most unstable frequency according to LST, and an amplitude of $\epsilon_s = 10^{-3}$. The figure includes the non-linear production term that arises from the interaction of the sound wave with the base flow during the very first disturbance cycle (dashed line). In contrast to our first arguments above, the largest production appears around (S) and (R), i.e., where the streamwise gradients are largest. The minimum in between is at the maximal height of the bubble where the x-gradient is close to zero. After 20 disturbance cycles a fundamental disturbance has developed that exceeds the non-linear forcing inside the bubble and that grows to an amplitude above that of the sound wave. This disturbance is a Tollmien–Schlichting wave because it evolves according to LST. Upstream of the intersection with the non-linear forcing term it is hidden by the latter. Its actual origin is in the region between the inflow boundary and $x = 1$. This can be inferred from a comparison between the non-linear term (dashed line) with the amplification according to LST: If the forcing term would have been able to directly excite the TS-wave, the latter would have dominated starting from its source, because the linear growth rate is always much larger than the streamwise increase of the forcing term.

4.2 Flapping

Low frequency oscillations of the detaching boundary layer and the ensuing shear layer are called 'flapping' in the literature. Unfortunately, their physical reason is somewhat obscure.

The following mechanisms can be imagined:

Receptivity and instability of the bubble. Sometimes it is argued that a laminar separation bubble itself may act as a resonator with respect to low frequency, long wave length disturbances which should be of the size of the bubble length [4, 13, 39]. Wind-tunnel experiments have shown that such disturbances are responsible for a vortex shedding at frequencies lower than the instability frequency [4]. For large-enough bubbles it is possible that such a mechanism leads to a low-frequency oscillation of the separating shear layer, i.e., its flapping. In order to investigate this hypothesis we are planning to perform investigations with low-frequency forcing of the bubble. Unfortunately, according results are not yet available at present.

Interactions between transition and the mean flow. This idea is very closely related to our observations in subsection 3.5 above, where we observed that increasingly large disturbance amplitudes make the bubble shrink. A smaller bubble, however, is less unstable according to LST. Hence, it can be expected that those disturbances which approach the bubble at a later time will be somewhat less amplified, with the consequence that transition occurs further downstream. Later transition means a larger bubble, as shown above. Now the newly approaching disturbances will find a more unstable flow, stronger amplification, and hence earlier transition, i.e., the cycle of bubble growth and reduction will be closed. Maucher [20] has actually observed such a mechanism in his 2-D DNS (also in Rist & Maucher, 2002 [34]). In this observation the low frequency motion of the LSB was about 100 times smaller than the primary instability frequency.

Interactions with far-field boundaries. Such interactions can never be fully ruled out in a restricted environment, either wind tunnel or DNS. In the first case there is the possibility of reflections at the physical walls in the second at the boundaries of the computational domain which are artificially introduced. In addition to these, the whole wind tunnel, the test section, or the whole set-up may oscillate because of resonance. Consequently, existing experimental investigations should be repeated in different facilities and numerical simulations should be performed using larger integration domains in order to get further indications for a possible presence or absence of such effects.

Careful investigations are needed to find the correct answer(s) to these hypothesises.

4.3 Short vs. Long Bubbles (Bubble Bursting)

In early LSB literature two kinds of laminar separation bubbles have been identified, *'short'* and *'long' bubbles*. The main difference between the two, apart from their streamwise length, is their influence on the pressure distribution of an airfoil. Short bubbles have a small, i.e., only a local influence, while large bubbles extend over a major part of the airfoil surface with according large impact mainly on the lift of the airfoil. For varying angle of attack the transition of the first to the second can be found in experimental data, as shown in Fig. 26 which is based on measurements from McCullough & Gault (1951) [24]. For low angles of attack a short laminar separation bubble develops very close to the leading edge. This can be detected by looking for flow separation and re-attachment at the wall and the characteristic short plateau-like pressure in between. As the angle of attack is increased the separation point (S) moves towards the nose because the stagnation point moves back on the underside of the section and because of the increasing pressure gradient. The re-attachment point (R) follows because transition occurs earlier when dp/dx becomes larger. Then, all of a sudden, as the angle of attack is increased beyond a certain threshold, (R) moves downstream and the suction peak drops down

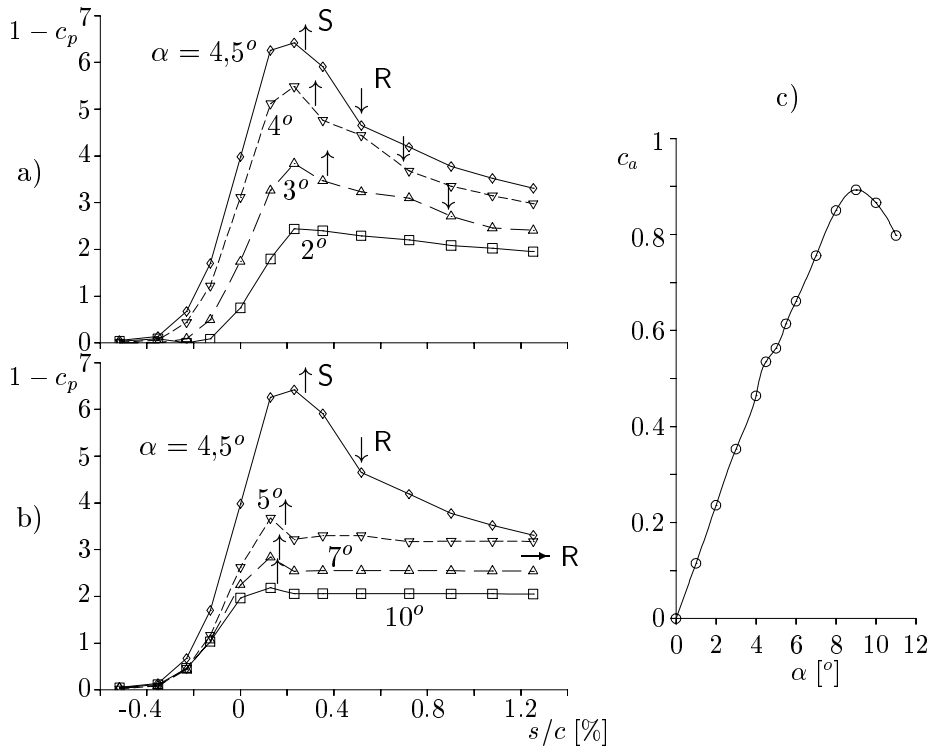

Figure 26: Pressure in the vicinity of the nose of a NACA 64A006 wing section (a, b) and lift coefficient (c) for varying angle of attack α and $Re = 5{,}8 \cdot 10^6$ according to McCullough & Gault (1951) [24]; S, ↑= separation; R, ↓ = re-attachment.

in a dramatic manner, see Fig. 26 b). However, for the present airfoil, lift is not immediately affected, as can be seen in Fig. 26 c) where only a small kink appears at $\alpha \approx 5^o$. Nevertheless, the maximal lift is attained when (R) reaches the trailing edge. From the investigations above it should be clear that an accurate prediction of a "long bubble" is a very difficult task because its length must be highly sensitive to initial disturbances and small errors in predicting transition and the ensuing flow. Typically there is also a hysteresis in such a way as two different bubble sizes or pressure distributions can be observed for the same angle of attack depending on whether the angle of attack has been previously increased or decreased. A similar effect is known from active separation control, depending on the fact whether control is used to delay separation or whether it is used to re-attach an already separated boundary layer.

Gaster [9] has tried to parameterize the occurrence of 'short' and 'long' bubbles based on wind-tunnel data. There is a good separation between the two, but it is not clear whether his empirical condition can be applied to free-flight conditions. There have been speculations that the transition from a short to a long bubble, termed *"bubble bursting"*, might be due to an absolute instability, e.g. [1]. However, in light of the results described above, it is also possible that this is not necessary, because it suffices that the turbulent flow doesn't reach the surface due to minor changes in angle of attack or in inflow disturbance amplitudes. Strictly speaking, yet, this is only a hypothesis at present that remains to be proven.

5.0 CONCLUSIONS AND OUTLOOK

Several basic mechanisms related to instability and transition in laminar separation bubbles have been isolated and studied. As far as possible, the present DNS results have been verified by comparisons with LST, experiments and grid refinement studies. Thus, it turned out that extreme care must be taken to reduce background disturbances because these must be controlled when trying to identify the mechanisms at hand. Also, the overall size of the bubble appeared to be very sensitive to small-amplitude disturbances and its mean-flow parameters exhibit large variations which would become unpredictable if the disturbance amplitudes were not known. The border between absolute and convective instability was revisited and further refined in terms of Reynolds number and thickness of the reverse-flow zone. Secondary instability and oblique breakdown were compared with the aim to identify the most relevant mechanism for amplification of three-dimensional disturbances. For large Reynolds numbers a new kind of secondary instability was found which leads to temporal growth of 3-D disturbances on the basis of a large-amplitude shear layer oscillation, regardless whether this is produced by an exactly 2-D TS-wave or by weakly oblique waves.

Many systematic hot-wire measurements of laminar separation bubbles have been performed by [9, 7, 43, 28, 41, 12], and others in order to identify the instability and transition mechanisms. However, it is difficult to get an equally complete picture of the flow physics from these as in the DNS presented here, because of the limitations of a single probe, the inability to completely control the disturbance background, and possible influences from introducing a probe into the bubble. A new area of non-intrusive measurement techniques has just begun with the arrival of LDV (Laser-Doppler Velocimetry) and PIV (Particle Image Velocimetry). These methods have the potential to yield an equally rich view into flow details like the present DNS. Comparisons of ongoing experiments with the present results indicate good agreement of the unsteady disturbance development, once the initial amplitudes have been found by iteration, because they cannot be measured directly due to their small initial amplitudes.

Summarizing the results shown above, it appears that the primary instability of most pressure-induced laminar separation bubbles is of convective nature. As a consequence, one should be warned, not to neglect the influence of the background disturbance spectrum, regardless of its smallness and despite additional accuracy improvements of the measurements. The point is that 'typical' mean-flow characteristics, like the position of separation, transition, reattachment, or the length of the bubble are governed by subtle flow physics, which are usually ignored, especially when experiments or computer simulations (e.g. RANS, LES, or DNS) are performed for mutual validation.

References

[1] M. Alam, N.D. Sandham (2000): Direct numerical simulation of 'short' laminar separation bubbles with turbulent reattachment, J. Fluid Mech. 410, May 2000, pp. 1–28

[2] T. Allen, N. Riley (1995): Absolute and convective instabilities in separation bubbles, Aeron. J. Royal Aeron. Soc., Dec. 1995, 439–448.

[3] D. Althaus (1981): Drag measurements on airfoils, XVII OSTIV-Kongress, Paderborn.

[4] A.V. Boiko, G.R. Grek, A.V. Dovgal, V.V. Kozlov (2001): Origin of turbulence in near-wall flows, Springer-Verlag, Berlin, Heidelberg.

[5] M. Choudhari (1993): Boundary-layer receptivity due to distributed surface imperfections of a deterministic or random nature, Theoret. Comput. Fluid Dynamics 4, 101–117.

[6] J.D. Crouch (1992): Localized receptivity of boundary layers, Phys. Fluids A 4 (7), 1408–1414.

[7] Dovgal, A.V., Kozlov, V.V., Michalke, A. (1994): Laminar boundary layer separation: Instability and associated phenomena, Progr. Aerospace Sci. 30, 61–94.

[8] H. Fasel, U. Rist, U. Konzelmann (1990): Numerical investigation of the three-dimensional development in boundary layer transition, AIAA J. 28 (1), 29–37.

[9] M. Gaster (1966): The structure and behaviour of laminar separation bubbles, AGARD CP-4, Flow separation, part II, 813–854.

[10] M. Gaster (1968): Growth of disturbances in both space and time, Phys. Fluids 11 (4), 723–727.

[11] M. Gaster (1991): Stability of velocity profiles with reverse flow, in: M.Y. Hussaini, A. Kumar, C.L. Streett (Eds.), Instability, Transition and Turbulence, ICASE-Workshop, Berlin, Springer, 212–215.

[12] C.P. Häggmark, C. Hildings, D.S. Henningson (2000): A numerical and experimental study of a transitional separation bubble, Aerosp. Sci. Technol. 5, 317-328.

[13] D.A. Hammond, L.G. Redekopp (1998): Local and global instability properties of separation bubbles, Eur. J. Mech. B/Fluids 17 (2), 145–164.

[14] T. Herbert (1988): Secondary instability of boundary layers, Ann. Rev. Fluid Mech. 20, 487–526.

[15] P. Huerre, P.A. Monkewitz (1985): Absolute and convective instabilities in free shear layers J. Fluid Mech. 159, 151-168.

[16] G.R. Inger (1986): A theoretical study of spanwise-periodic 3D disturbances in the wake of a slightly stalled wing at low Reynolds numbers, Aerodynamics at Low Reynolds Numbers $10^4 < Re < 10^6$, Royal Aeronautical Society, London, Oct. 1986.

[17] M. Kloker, U. Konzelmann, H. Fasel (1993): Outflow boundary conditions for spatial Navier–Stokes simulations of transitional boundary layers, AIAA J. 31 (4), 620–628.

[18] M. Lang, O. Marxen, U. Rist, S. Wagner (2001): Experimental and numerical investigations on transition in a laminar separation bubble, in: S. Wagner, U. Rist, H.J. Heinemann, R. Hilbig (Eds.), New Results in Numerical and Experimental Fluid Mechanics III, Proc. 12. DGLR-Fachsymposium AG STAB, Stuttgart, 15.–17.11.2000, NNFM Vol. 77, Springer-Verlag, 194–201.

[19] M. Lang, U. Rist, S. Wagner (2002): Investigation on disturbance amplification in a laminar separation bubble by means of LDA and PIV, Proc. 11th Int. Symp. Appl. Laser Tech. Fluid Mech., 8.–11. July, Lisbon, Portugal.

[20] U. Maucher (2001): Numerische Untersuchungen zur Transition in der laminaren Ablöseblase einer Tragflügelgrenzschicht, Dissertation Universität Stuttgart.

[21] U. Maucher, U. Rist, M. Kloker, S. Wagner (2000): DNS of laminar-turbulent transition in separation bubbles, in: E. Krause, W. Jäger (Eds.), High Performance Computing in Science and Engineering '99, Springer-Verlag, Berlin, Heidelberg, pp. 279–294.

[22] U. Maucher, U. Rist, S. Wagner (1999): Transitional structures in a laminar separation bubble, in: W. Nitsche, H.J. Heinemann, R. Hilbig (Eds.), New Results in Numerical and Experimental Fluid Mechanics II, NNFM Vol. 72, Vieweg, Braunschweig, 307–314.

[23] U. Maucher, U. Rist, S. Wagner (2000): A refined interaction method for DNS of transition in separation bubbles, AIAA J. 38, 1385–1393.

[24] G.B. McCullough, D.E. Gault (1951): Examples of three representative types of airfoil-section stall at low speed, NACA TN 2502.

[25] A. Michalke (1965): On spatially growing disturbances in an inviscid shear layer, J. Fluid Mech. 23, 521–544.

[26] A. Michalke (1990): On the inviscid instability of wall-bounded velocity profiles close to separation, ZFW 14, 24–31.

[27] A. Michalke, V.V. Kozlov, A.V. Dovgal (1995): Contribution to the instability of laminar separating flows along axisymmetric bodies. Part I: Theory, Eur. J. Mech. B/Fluids 14 (3), 333–350.

[28] D.M. Paschier (1997): Hot-wire measurements in the neighbourhood of a laminar separation bubble, in: R.A.W.M. Henkes and P.G. Bakker (Eds.) *Boundary-Layer Separation in Aircraft Aerodynamics*, Delft University Press, Delft, The Netherlands, 69–86.

[29] U. Rist (1994): Nonlinear Effects of 2-D and 3-D disturbances on laminar separation bubbles, *in:* S.P. Lin, W.R.C. Phillips, D.T. Valentine (Eds.): *Proc. IUTAM-Symp. Nonlin. Instab. of Nonpar. Flows*, Potsdam, NY/USA 1993, Springer-Verlag, 330–339.

[30] U. Rist (1999): Zur Instabilität und Transition in laminaren Ablöseblasen, Habilitation Universität Stuttgart, Shaker, Aachen, Maastricht, 1999.

[31] U. Rist, K. Augustin (2003): Control of laminar separation bubbles, VKI/RTO-LS "Low Reynolds Number Aerodynamics on Aircraft Including Applications in Emerging UAV Technology", Rhode-Saint-Genèse, Belgium, 24–28 November 2003

[32] U. Rist, H. Fasel (1995): Direct numerical simulation of controlled transition in a flat-plate boundary layer, J. Fluid Mech. 298, 211–248.

[33] U. Rist, U. Maucher (1994): Direct numerical simulation of 2D and 3D instability waves in a laminar separation bubble, AGARD CP-551, Application of Direct and Large Eddy Simulation to Transition and Turbulence, Chania, Crete, 34-1–34-7.

[34] U. Rist, U. Maucher (2002): Investigations of time-growing instabilities in laminar separation bubbles, European Journal of Mechanics B/Fluids 21, 495–509.

[35] U. Rist, U. Maucher, S. Wagner (1996): Direct numerical simulation of some fundamental problems related to transition in laminar separation bubbles, in: J.-A. Désidéri, C. Hirsch, P. Le Tallec, M. Pandolfi, J. Périaux (Eds.), Computational Fluid Dynamics '96, John Wiley & Sons, Ltd., 319–325.

[36] H. Schlichting, K. Gersten, C. Mayes (Translator) (2000): Boundary-Layer Theory, Springer-Verlag New York.

[37] C. Stemmer (1995): Numerische Simulation zum Einfluš einer ebenen Schallwelle auf eine Grenzschicht mit und ohne Ablöseblase, Diplomarbeit Universität Stuttgart, Institut für Aerodynamik und Gasdynamik.

[38] I. Tani (1964): Low-speed flows involving bubble separations, Progr. Aeron. Sciences 5, 70–103.

[39] V. Theofilis (2003): Advances in global linear instability analysis of nonparallel and three-dimensional flows, Progress in Aerospace Sciences 39 (4), 249–315.

[40] A.E.P. Veldman (1981): New, quasi-simultaneous method to calculate interacting boundary layers, AIAA J. 19, 79–85.

[41] J.H. Watmuff (1999): Evolution of a wave packet into vortex loops in a laminar separation bubble, J. Fluid Mech. 397, 119–169.

[42] F.M. White (1991): Viscous Fluid Flow, Second Edition, McGraw-Hill, New York.

[43] W. Würz (1997): Experimental investigations of transition development in attached boundary layers and laminar separation bubbles, in: H. Körner, R. Hilbig (Eds.), New Results in Numerical and Experimental Fluid Mechanics, 10. AG STAB/DGLR Symposium 1996, NNFM 60, Vieweg, Braunschweig, 413–420.